Volume 8 | Number 30 | 14 August 2016 | Pages 14283–14684

Nanoscale

www.rsc.org/nanoscale

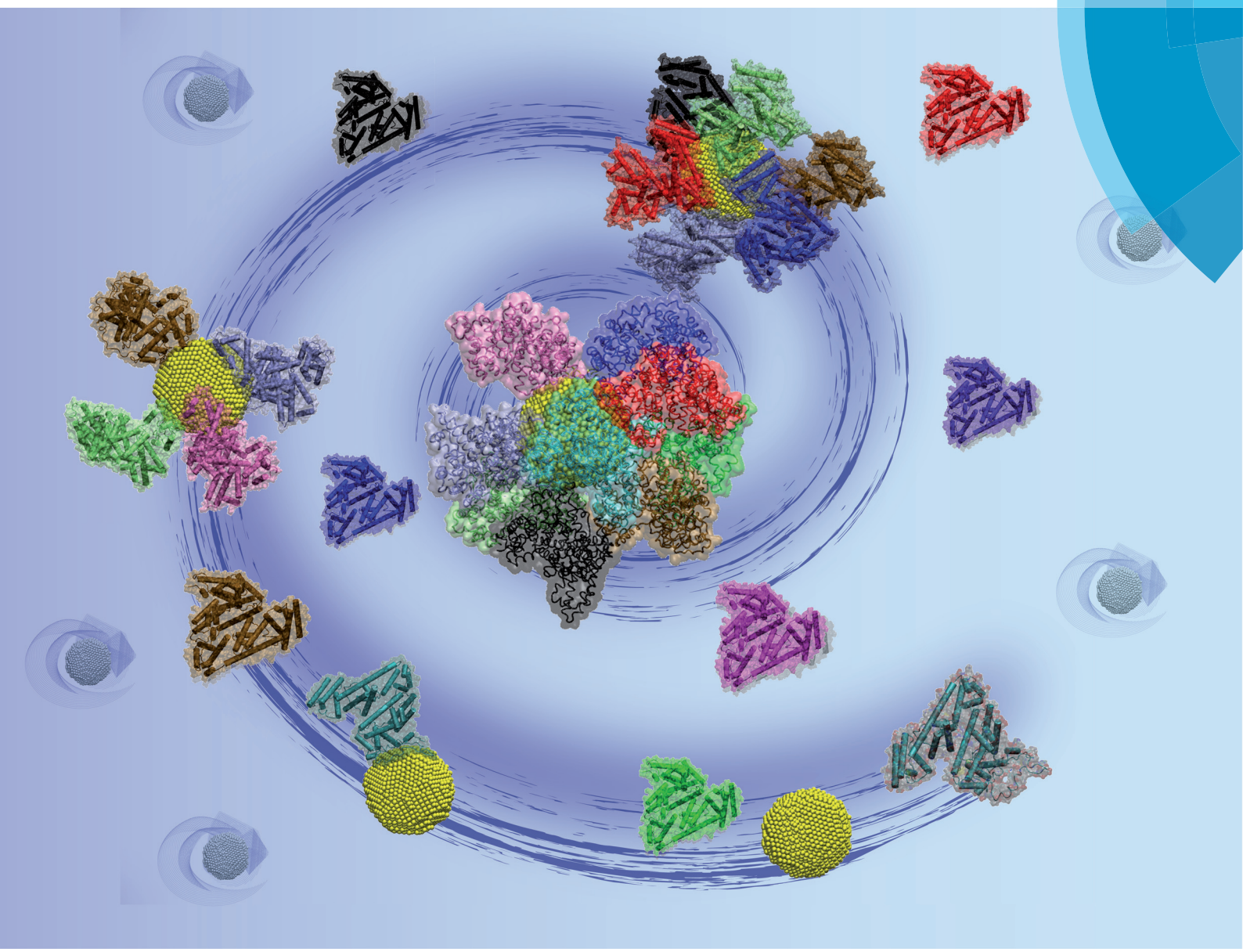

ISSN 2040-3364

ROYAL SOCIETY OF CHEMISTRY

PAPER

Anna Roig, Anna Laromaine *et al.*

Albumin-coated SPIONs: an experimental and theoretical evaluation of protein conformation, binding affinity and competition with serum proteins

NCNST

Nanoscale

PAPER

View Article Online
View Journal | View Issue

Cite this: *Nanoscale*, 2016, **8**, 14393

Albumin-coated SPIONs: an experimental and theoretical evaluation of protein conformation, binding affinity and competition with serum proteins†

Siming Yu,[a] Alex Perálvarez-Marín,[b] Caterina Minelli,[c] Jordi Faraudo,[a] Anna Roig*[a] and Anna Laromaine*[a]

Received 29th February 2016,
Accepted 23rd May 2016

DOI: 10.1039/c6nr01732k

www.rsc.org/nanoscale

The variety of nanoparticles (NPs) used in biological applications is increasing and the study of their interaction with biological media is becoming more important. Proteins are commonly the first biomolecules that NPs encounter when they interact with biological systems either *in vitro* or *in vivo*. Among NPs, super-paramagnetic iron oxide nanoparticles (SPIONs) show great promise for medicine. In this work, we study in detail the formation, composition, and structure of a monolayer of bovine serum albumin (BSA) on SPIONs. We determine, both by molecular simulations and experimentally, that ten molecules of BSA form a monolayer around the outside of the SPIONs and their binding strength to the SPIONs is about 3.5×10^{-4} M, ten times higher than the adsorption of fetal bovine serum (FBS) on the same SPIONs. We elucidate a strong electrostatic interaction between BSA and the SPIONs, although the secondary structure of the protein is not affected. We present data that supports the strong binding of the BSA monolayer on SPIONs and the properties of the BSA layer as a protein-resistant coating. We believe that a complete understanding of the behavior and morphology of BSA-SPIONs and how the protein interacts with SPIONs is crucial for improving NP surface design and expanding the potential applications of SPIONs in nanomedicine.

Introduction

The use of nanoparticles (NPs) for medicine is becoming a key technology. The development of NPs for a broad range of activities and with multifunctional properties is blooming. The successful commercialization of these NPs is limited due to a lack of control and prediction of the final NP properties, which decide the way NPs interact with the environment and their ultimate fate.[1,2]

Proteins are commonly the first biomolecules that NPs encounter when they interact with biological systems either *in vitro* or *in vivo*. The adsorption of proteins on the surface of NPs leads to changes in the conformation and biological activity of the proteins, and modifies the designed properties of the NPs,[3–5] which can subsequently affect *in vitro* or *in vivo* biological responses.[6–9] The ability to develop NPs with protein-resistant coatings can impact the development of efficient drug-delivery systems with specific targeting strategies. Different strategies have been developed; for instance, using polyethylene glycol (PEG),[10] which prevents protein adsorption, confers stability to the NPs, decreases the uptake of NPs by culture cells *in vitro*[11,12] and by entire organisms *in vivo*,[13] and increases their retention time in blood flow. However, some studies found that PEG can be oxidized by enzymes and some proteins still adsorb on to it.[10,14,15]

Natural products as bovine serum albumin (BSA) are also exploited to form a protective layer on the NPs to improve biocompatibility and transport of the NPs;[16] for instance, novel commercial drugs, such as Abraxane, incorporate albumin in the drug formulation to efficiently accumulate the drug in the tumor due to an enhanced permeability and retention and to reduce the risk of hypersensitivity reactions. Drug release in albumin carriers can be triggered naturally by protease digestion or pH-responsive systems; the payload can be

[a]*Institut de Ciència de Materials de Barcelona (ICMAB-CSIC), Campus UAB, 08193 Bellaterra, Spain. E-mail: roig@icmab.es, alaromaine@icmab.es*
[b]*Unitat de Biofísica, Departament de Bioquímica i de Biologia Molecular, Universitat Autònoma de Barcelona, 08193 Bellaterra, Spain*
[c]*Analytical Science, National Physical Laboratory, Hampton Road, TW110LW Teddington, UK*

†Electronic supplementary information (ESI) available. See DOI: 10.1039/c6nr01732k

tuned by the amount of albumin on the NPs, and the unfolding of the protein on the NP can facilitate their clearance by phagocytes.[17] Additionally, BSA maintains the colloidal stability of the NPs and it is a standard additive in the serum used in cell-culture experiments. Because of these properties, BSA seems a good coating candidate to obtain biocompatible and protein-resistant NPs.

The US Food and Drug Administration approved the use of super-paramagnetic iron oxide nanoparticles (SPIONs) in the 1990s as nuclear magnetic resonance imaging contrast agents, and they hold great promise for applications in magnetic separation, cell targeting, imaging, and in drug-delivery systems.[18–20]

The potential of SPIONs for biomedical applications, and the benefits of albumin coatings, lead us to investigate how BSA interacts with SPIONs (BSA-SPIONs; Scheme 1) and how it can improve SPIONs' performance. Different strategies have been published using covalent or non-covalent immobilization of BSA on SPIONs. Strategies to covalently anchor BSA require the modification of the initial SPIONs with tedious reactions with organic solvents (toxic for biological applications), the exchange of solvents and they restrict and fix the conformation of the anchored protein.[16,21] Non-covalent strategies require hydrophilic iron oxide surfaces, the common method of synthesis cannot offer it; and it adds an extra step.[16,17] In our case, we synthesized SPIONs using microwave-assisted thermal decomposition and capped them with citrate, rendering hydrophilic SPIONs in a single step. Both strategies, covalent and non-covalent, afford more biocompatible and colloidally stable SPIONs systems and confirm the formation of a hard corona on the SPIONs surfaces. We chose non-covalent interaction for its practicality and efficiency. Here we study bovine albumin coated SPIONs (BSA-SPIONs) in detail by using a broad range of techniques; we also evaluate the binding strength of BSA on SPIONs and the potential of BSA coating to resist serum–protein adsorption by using isothermal titration calorimetry and gel electrophoresis. A complete understanding of the behavior and morphology of BSA-SPIONs and how the protein interacts with SPIONs are crucial for improving NPs surface design and expanding the potential applications of SPIONs in nanomedicine.

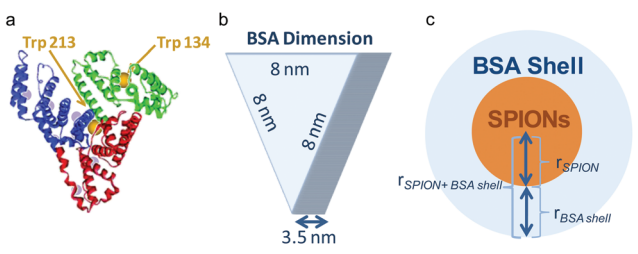

Scheme 1 (a) Crystal structure of BSA where the position of the tyrosine (gray spheres) and tryptophan (labeled) residues are highlighted. (b) Scheme of the dimensions of the BSA as an equilateral triangular prism. (C) Schematic of the BSA-SPION complex.

Methods

Chemicals and materials

Iron(III) acetylacetonate ($Fe(acac)_3$, ≥97.0%), trisodium citrate dihydrate (citrate), and bovine serum albumin (BSA, ≥98%, Sigma, A7906-50G), phosphate-buffered saline (PBS, P5493-1L) 10× was diluted before use were purchased from Sigma-Aldrich and used as received. Fetal bovine Serum (FBS, 10270106) was bought from Life Technologies.

Protocol for the preparation of bovine serum albumin coated SPIONs (BSA-SPIONs) are described previously in detail.[22] In brief, SPIONs were synthesized by microwave-assisted thermal decomposition of the iron precursor and then coated with citrate in a single step, to obtain citrate-coated SPIONs (C-SPIONs). This approach produced monodisperse C-SPIONs in just 15 min. Transmission electron microscopy (TEM) revealed that C-SPIONs are spherical with a diameter of 6 ± 1 nm. Dynamic light scattering (DLS) indicated a hydrodynamic diameter (D_h) of 15 ± 1 nm in water, while the ζ-potential was −36 mV and a saturated magnetization of 62 emu g^{-1} was measured at room temperature by magnetometry.[22] BSA was adsorbed on the C-SPIONs' surface by using a pH-adjusted protocol, which significantly improved the stability of C-SPIONs in a wide range of biological media.[16,22] C-SPIONs in water were adjusted to pH 11 with 0.1 mM NaOH and then BSA was incubated with them at this pH for 1 h. Subsequently, the system was neutralized to pH 7.4 with 0.6 mM HNO_3 and the excess BSA was removed by centrifugation for all the experiments, (Fig. S1†). Hereafter, we will refer to this system as BSA-SPIONs.

BSA-SPIONs used in this work were all purified if not stated otherwise; purification followed the protocol: the obtained BSA-SPIONs dispersions were transferred to a centrifugal filter unit (Amicon, 100 000 MW, Millipore), centrifuged at 2548*g* for 25 min to remove the unbound BSA. The removed supernatant was collected and UV-vis spectra were recorded. The concentrated BSA-SPIONs were then redispersed in MilliQ water and filtered again under the same conditions. The filtration and centrifugation steps were repeated several times until the supernatant showed no UV-vis absorption at 280 nm. In our case, after three washing steps, UV-vis spectra of the isolated solution did not show any absorption at 280 nm (Fig. S2a†), which indicates the complete removal of free BSA from the BSA-SPIONs dispersion. The purified BSA-SPIONs were characterized further.

Characterization

C-SPIONs and BSA-SPIONs solutions. Stock solutions of 100 μM C-SPIONs and 100 μM BSA-SPIONs purified in PBS were used as starting solutions to perform the following analysis.

X-ray photoelectron spectroscopy (XPS). Samples for XPS investigation were prepared by depositing drops of 11.6 mg mL^{-1} concentrated solution of NPs onto a 1 × 1 cm^2 polytetrafluoroethylene-wrapped silicon wafer. Aliquots of 5 μL

were applied and allowed to dry under vacuum in a desiccator before the addition of the next aliquot on top of each spot. This process was repeated until uniform coverage of the surface was achieved, typically for a total of 50–100 μL. Samples were prepared in triplicate.

XPS spectra were acquired using an Axis-Ultra XPS instrument (Kratos Analytical, Manchester, UK) with monochromatic Al K_α X-rays (15 kV, 5 mA) in hybrid lens mode. Survey scans (single sweep) were acquired with a pass energy of 160 eV, step size 1000 meV, and a dwell time of 300 ms. Narrow scans were performed for the Fe 2p, C 1s, N 1s, O 1s, S 2p, and F 1s regions with a pass energy of 40 eV, step size 100 meV and a dwell time of 500 ms. Two sweeps were acquired for each of the narrow scan regions except for iron, carbon, and nitrogen, for which four sweeps were obtained. Charge neutralization was employed to reduce charging of the samples, and balance settings were determined on an individual basis. XPS spectra were analyzed by using CasaXPS software (Version 2.3.16) and intensities were calibrated with the NPL's (National Physical Laboratory) own transmission function and average matrix relative sensitivity factors. Tougaard backgrounds were used for peak quantification, except for a minority of cases where linear background was used instead.

Dynamic light scattering (DLS). Hydrodynamic diameter (D_h) and Polydispersity index (PDI) of samples were determined by using a Zetasizer Nano ZS (Malvern) equipment with a He/Ne 633 nm laser at 25 °C. For each sample, three independent measurements were performed with 15 scans for each measurement. All samples had a concentration of SPIONs of 50 μg mL^{-1}. Results are plotted as size average from the intensity measurements on the DLS plot. Table S1† summarizes D_h and PDI of the samples.

Zeta potential (ζ-potential) was carried out on a Zetasizer Nano ZS (Malvern) apparatus with a zeta potential analyzer software. C-SPIONs (50 μg mL^{-1}) solutions were placed in a disposable plastic cuvette, followed by collecting experimental data automatically using the built-in software. For each measurement, 20 cycles were collected, and at least 3 independent measurements were performed for each sample.

Transmission electron microscopy (TEM). A drop of sample solutions was added to the TEM copper grid, the excess blotted with a filter paper and then evaporated completely at room temperature. SPIONs were imaged in a JEOL TEM-1210 electron microscope at an operating voltage of 120 kV. A size-distribution histogram of SPION samples was computed from over 200 NPs and fitted to a Gaussian function to obtain NP mean size using ImageJ software. Selected-area electron diffraction (SAED) was used to identify the crystallographic phase of the NPs.

Negative-staining TEM. Adsorption of BSA on C-SPIONs were visualized by performing negative-staining TEM. Briefly, one drop of the purified BSA-SPIONs was placed on a carbon-coated grid and blotted with filter paper. Subsequently, 5 μL of 2% uranyl acetate was placed on the grid for 1 min before draining off. The grid was then placed in a 2011 JEOL electron microscope under the working voltage of 100 kV.

UV-visible spectroscopy (UV-vis). UV-vis extinction spectra of the samples were collected on a Cary-5000 UV-Vis spectrophotometer at room temperature. Each sample was prepared starting from the stock solutions to 4 μM BSA and a concentration of SPIONs ranging from 0–72 μM in 10 mM PBS (pH 7.4). Each UV-vis spectrum was the average of three scans; three independent measurements were performed. The UV-vis spectrum of BSA displays two characteristic adsorption peaks, at 220 and at 280 nm. The strong adsorption peak at 220 nm is assigned to the transition of π–π* of the polypeptide backbone structure C═O of BSA, while the one at 280 nm is due to aromatic amino acid residues such as tryptophan (Trp), tyrosine (Tyr), and phenylalanine (Phe).[4]

Determination of the saturated BSA adsorption number. The 280 nm peak shows a linear correlation between its intensity and BSA concentration (Fig. S2b†). Thus, UV-vis spectroscopy was used to quantify the amount of BSA adsorbed on the C-SPIONs surface by measuring UV absorption at 280 nm and subtracting the unbound BSA present in the supernatant from the adsorption of the initial known amount of BSA. This calculation resulted in a value of 1.8 ± 0.2 mg BSA per mg SPIONs, which corresponds to approximately 10 ± 1 BSA molecules per iron oxide NP. The ten BSA molecules can be considered to form a hard corona since loosely bound BSA was removed during filtration and centrifugation steps.

Fluorescence quenching measurements. Fluorescence measurements were performed on a fluorescence spectrophotometer (HITACHI F-7000, Japan) at 25 °C, in a 1 cm-path length rectangular quartz cell. All the emission spectra were collected at the excitation wavelength of 295 nm using 10 nm per 10 nm (excitation/emission) slit widths. Each spectrum is the average of at least three scans. Each sample was prepared starting from the stock solutions to the final 4 μM BSA and the concentration of SPIONs ranging from 0–72 μM in 10 mM PBS (pH 7.4). Duplicate measurements were performed for each SPION concentration. Fluorescence backgrounds were corrected for blank buffer solutions in each measurement.

Equation F_o/F *vs.* [SPIONs] were represented in logarithmic form, and a sigmoidal curve was fitted to the data, to give the equation:

$$y = A_2 + \frac{(A_1 - A_2)}{1 + \left(\frac{X}{X_o}\right)^p}$$

$Ch^2/D_oF = 0.0056$; $r^2 = 0.99745$; $A_1 = 1.04 \pm 0.045$; $A_2 = 172 \pm 188.2$; $X_o = 8.6 \times 10^{-4} \pm 6.52 \times 10^{-3}$; $p = 1.55 \pm 0.24$.

Circular dichroism spectroscopy (CD). CD measurements were recorded on a Jasco J-810 spectro-polarimeter (Easton, MD) with a 0.1 cm-path length of cylindrical quartz cell at room temperature, with a fixed BSA concentration of 4 μM. The CD spectra were recorded from 200–260 nm, and each

spectrum was an average of three scans. Each sample was prepared starting from the stock solutions to the final 4 μM BSA and the concentration of SPIONs ranging from 0–72 μM in 10 mM PBS (pH 7.4).

Data was fitted by using the software described in http://cbdm-01.zdv.uni-mainz.de/~andrade/k2d3/.[23]

Isothermal titration calorimetry (ITC). Isothermal titration calorimetry measurement was performed on a VP-ITC calorimeter (Microcal Inc., Northampton, MA) at room temperature (25 °C). For titration of BSA to C-SPIONs, BSA was dialyzed extensively against 10 mM sodium phosphate buffer and the C-SPIONs were dispersed in the last dialysate. Both solutions were at pH 7.4. A typical titration experiment involved 26 injections of the titrant BSA solution (10 μL aliquot per injection from a 0.5 mM stock BSA solution) at 210 seconds intervals into the sample cell (volume of 1.44 mL) containing 8 μM C-SPIONs. During the experiment, the sample cell was stirred continuously at 1000 rpm. The heat released on BSA dilution in the buffer was subtracted from the titration data for each experiment. Titration of fetal bovine serum (FBS) to C-SPIONs and BSA-SPIONs followed the same protocols as described above. The data collected were fitted and analyzed by using the one set binding model coupled in Origin software with the ITC system, to provide thermodynamic parameters of enthalpy (ΔH), binding stoichiometry (n), and affinity constant (K_a). Other thermodynamic parameters were calculated accordingly. The obtained thermodynamic parameters were an average of duplicate experiments.

Superconducting quantum interference device (SQUID). The magnetic characterization was performed with a Quantum Design MPMS5XL Magnetometer. 150 μL of C-SPIONs of 11.6 mg mL^{-1} were first dried in a polycarbonate capsule at 60 °C overnight and then transferred to the SQUID sample holder. Magnetization curves of SPIONs at 5 K were recorded as a function of applied magnetic field up to 6 T.

Flame absorption spectroscopy. To determine the iron concentration of C-SPIONs, samples were sonicated for 10 min in an ultrasound bath. An aliquot of the sample was diluted with HCl (1%) and the iron content of the resulting solution was determined by flame absorption spectroscopy (air–acetylene) with a Perkin-Elmer 2100 spectrometer in a triplicate essay.

Gel electrophoresis experiments. Samples were diluted in Laemli buffer and heated at 95 °C for 5 min prior to loading in a 10% sodium dodecyl sulfate-polyacrylamide gel electrophoresis (SDS-PAGE) gel. Electrophoresis was performed at 160 V for 90 min and gel was stained by using Commassie blue. Bands were quantified in ImageJ by integration of the area under the curve (AUC) corresponding to the BSA band (indicated). The relative fold for BSA binding corresponds to ratio between the protein-incubated SPIONs *versus* the SPION-alone conditions.

Methodology for computer simulations

Modeling and force fields. BSA proteins were modeled with atomistic resolution, by employing the CHARMM27 force field.[24] The BSA structure was obtained from the most recent X-ray crystallographic structure with 2.58 Å resolution (PDB code: 4OR0).[25] The X-ray structure was completed by adding the missing hydrogen atoms (H) with the VMD program[26] and minimizing the energy of the obtained structure by using the NAMD program.[27] The employed protonation states correspond to a neutral pH state. The obtained structure for a BSA protein has 9207 atoms. The effect of solvent was modeled by employing a generalized Born Implicit Solvent model (GBIS).[28] Detailed modeling of the complex C-SPIONs in detail was not attempted. Instead, we considered a simplified, generic model of a NP. In this model, the NP was a cluster of Lennard-Jones spheres, with parameters ϵ = 5.29 kcal mol^{-1} and R_{min} = 3.62 Å as employed previously for generic models of hydrophilic adsorbing surfaces.[29] An approximately spherical cluster of 6 nm was obtained with 4104 atoms.

Molecular dynamics (MD) simulations. All MD simulations were performed by using the NAMD 2.9 software. In these simulations the Newton equations of motion were solved numerically with a time-step of 2 fs. The temperature was kept constant at 298 K using the Langevin thermostat with a relaxation constant of 1 ps^{-1}. The parameters for the GBIS calculations in NAMD were the same employed in ref 28. We first performed MD simulations of a single BSA protein in implicit water. After that, we performed MD simulations of the adsorption of different numbers of BSA proteins onto a single NP. We first considered the adsorption of a single BSA and subsequently added more BSA proteins, to obtaining simulations with a single NP and 1, 2, 4, 8, 10, and 12 BSA proteins. The total simulation time was about 130 ns, although the kinetics observed for the proteins are not expected to correspond exactly to these time scales due to the use of implicit solvent. In GBIS implicit solvent, protein atomic motion and rearrangement is substantially accelerated.[28] The results were analyzed with the VMD program to obtain the solvent accessible surface area (SASA), the root-mean-square deviation of atomic positions (RMSD), and the α-helix content of BSA proteins during the simulations. Density profiles in the radial direction were obtained by using our own python code.

Results & discussion

Super-paramagnetic iron oxide NPs (SPIONs) were synthesized by microwaveassisted thermal decomposition of the iron precursor and then coated with citrate in a single step, to obtain citrate-coated SPIONs (C-SPIONs). BSA was adsorbed on the C-SPIONs' surface by using a pH-adjusted protocol (Fig. S1†), detailed synthesis and characterization were provided previously.[22] The excess BSA was removed by centrifugation for all the experiments. Hereafter, we will refer to this system as BSA-SPIONs.

BSA shell formation

By using DLS, we monitored the increase of D_h of C-SPIONs upon BSA incubation at room temperature for 1 h for concen-

trations ranging from 0.1–100 μM BSA. DLS exhibits a slight increase in D_h at low BSA concentrations, and a sharp increase of D_h in the range of 1–20 μM BSA, which reaches a plateau at D_h = 23 nm for 20–50 μM BSA (Fig. 1a). Mean values and polydispersity are gathered in Table S1.† We infer that a concentration of 20 μM is sufficient to saturate the surface of the C-SPIONs with BSA. Additionally, the appearance of a peak in the DLS size distribution at 8 nm suggests the presence of free BSA in solution at 30 μM BSA, which supports the hypothesis of a saturated BSA coating on the NPs (Fig. 1b). Fig. S3† presents the DLS size distribution of only BSA. The difference of the hydrodynamic diameter value at the plateau ($D_{h\_plateau}$) of BSA-SPIONs and the D_h value of C-SPIONs is 7 nm, which corresponds to a radius of 3.5 nm, and therefore a hydrodynamic-shell thickness of about 3.5 nm; indicative of a monolayer of BSA.[17,22]

Negative-staining TEM of BSA-SPIONs was previously reported by us and it showed that the BSA shell on the SPIONs measured 3 ± 1 nm thick (Fig. 1c).[22]

BSA shell composition

To estimate the composition of the shell, we performed XPS of C-SPIONs and BSA-SPIONs and we identified all the expected elements in the system, Fig. 2 and S4.† The BSA-SPIONs C 1s spectrum exhibits a peak shoulder at 286 eV, which is characteristic of the N–C bond arising from BSA,[30] and it is therefore present in the BSA-SPIONs and not in the C-SPIONs. Consistently, nitrogen was only detected in the BSA-SPIONs, as shown by the N 1s high resolution spectra in Fig. S4c.† Once we subtracted the contribution of the NP iron oxide core to the XPS signal, we computed the average relative elemental composition of the NP shell and compare it to that of pure BSA (Fig. 2c). Assuming that BSA is the only N-containing molecule in the shell, we estimated that 74% of the shell is covered by BSA. The higher level of C and lower level of N measured in the BSA-SPIONs' coating compared to pure BSA suggest the presence of additional carbonaceous species such as citrate. By FT-IR we detected in BSA-SPIONs the typical bands of citrate (red color in Fig. 2d) and BSA (gray color in Fig. 2d); their slight red-shift indicates an interaction with the SPIONs. The detection of the citrate bands in the final BSA-SPIONs suggests the presence of sodium citrate as part of the shell, which indicates that BSA adsorbs on SPIONs' surface through the interaction with citrate rather than replacing it.

Number of bovine serum albumin molecules in the coating shell

Considering the BSA dimensions,[31] ≈8 × ≈8 × ≈3.5 nm^3, (Scheme 1) the measured thickness of the observed BSA layer by TEM we estimated the number of molecules present in the shell of the C-SPIONs by using eqn (1).

$$N = \frac{\frac{4}{3}\pi\left(r^3_{\mathrm{SPION+BSA\ shell}} - r^3_{\mathrm{SPION}}\right)}{V_{\mathrm{BSA}}} \quad (1)$$

where N is the number of BSA molecules per SPIONs; V_{BSA} is the BSA's volume (83 nm^3);[32] $r_{SPION+BSA\ shell}$ is the radius of the BSA-SPIONs core shell NPs; r_{SPION} is the measured radius of the SPIONs.

By taking the values obtained from the TEM, r_{SPION} = 3.0 nm; $r_{BSA\ shell}$ = 3.0 nm; we conclude that approximately 10 ± 2 molecules form the saturated BSA layer on our SPIONs. We confirmed this number by using UV-vis spectroscopy, where we computed the number of proteins constructing the BSA monolayer from the optical absorption measured on the particle supernatant after incubation. We obtained a value of ten molecules of BSA per SPION at saturation, which is in good agreement with our previous estimate.

To confirm these results; we ran molecular dynamics (MD) simulations with atomistic resolution. We simulated the protein shell on a NP of 6 nm diameter to compute the maximum theoretical number of albumin molecules that can be adsorbed onto the NPs. The simulations were done by systematically adding two BSA proteins in solution, from 2 up to 12 BSA molecules, and allowing the proteins to structurally

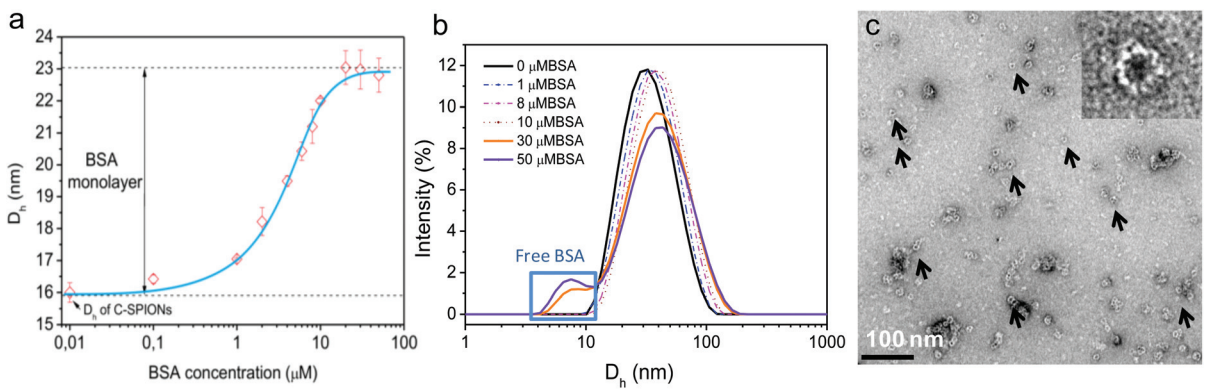

Fig. 1 (a) Hydrodynamic diameter (D_h) change upon absorption of BSA, error bars are the standard deviation determined from 3 independent measurements of 15 scans each. (b) Intensity-weighted D_h distribution curves of BSA-SPIONs prepared at different BSA concentrations. The blue square indicates the presence of excess BSA in solution, (c) negative-staining TEM image of BSA-SPIONs.

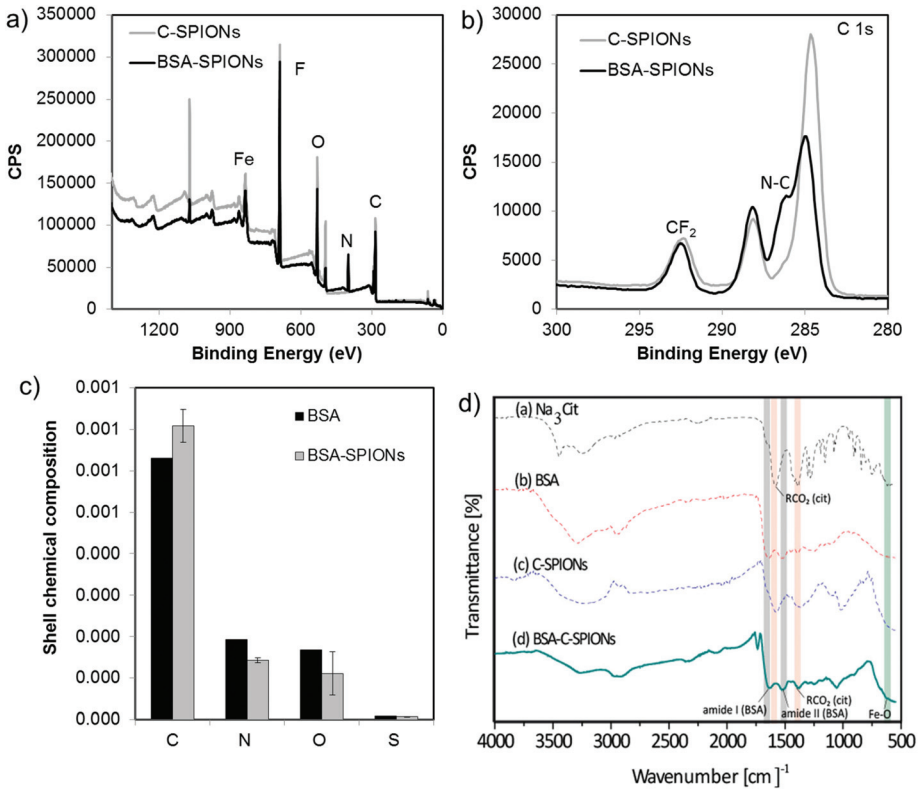

Fig. 2 XPS (a) survey and (b) C 1s spectra of C-SPIONs and BSA-SPIONs. (c) Relative elemental composition of the coating on the BSA-SPIONs (gray) and, for comparison, the expected composition for pure BSA (black). XPS measurements were performed in triplicate and the declared uncertainty is the resulting standard deviation. (d) FTIR spectra of BSA-SPIONs, C-SPIONs, BSA, and citrate.

relax and adsorb to the surface (see Methods section for details). In Fig. 3, we show snapshots of configurations of adsorbed proteins obtained in these simulations, which indicate that the maximum value of BSA proteins that can be accommodated onto the 6 nm NP is ten. For the simulation with 12 BSA molecules, two of the proteins remained in solution. This result also indicates that, even in excess in solution; BSA does not form a multilayer over the NP, in accordance with the results from DLS.

The structure of the protein adsorbed layer, containing ten BSA molecules, can be seen in Fig. 3a and b. The layer is relatively compact, with some of the adsorbed BSA proteins in close contact, but it has also small gaps between the proteins that fluctuate over time, and protrusions of protein groups at

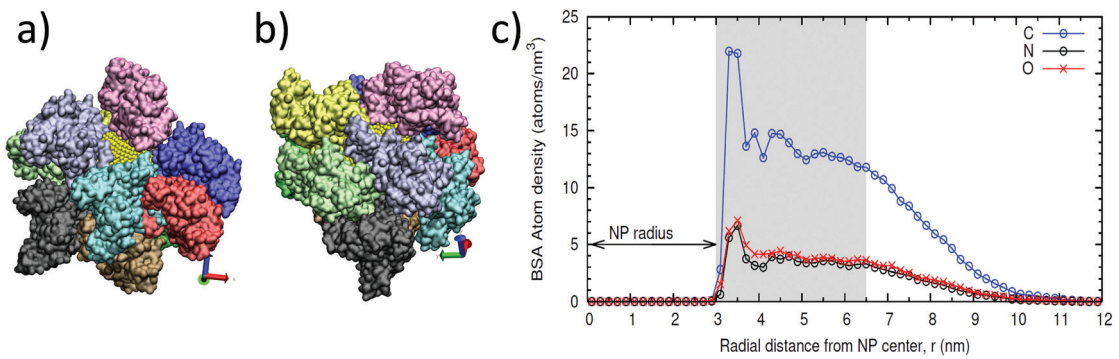

Fig. 3 Results from MD simulations with ten BSA proteins adsorbed onto a NP. (a, b) Snapshots of the same configuration with different orientation. The NP is shown in yellow, although only small patches of it can be seen due to the adsorbed protein corona. Proteins are shown in surface representation. Each protein is shown in a different color. (c) Radial density profile of C, N, and O atoms of BSA proteins. The shaded region corresponds to the more compact layer.

longer distances from the NP surface. This result can also be seen in the atomic density profile shown in Fig. 3c, which shows the time-averaged distribution of the C, N, and O atoms of the proteins in the adsorbed layer, measured from the center of the NP. There is a clear adsorption peak at $r \approx 3.5$ nm, which corresponds to atoms in close contact with the surface of the NP (radius is ≈3 nm). After this peak, there is a region with an accumulation of BSA (with an approximately constant density of O and N atoms) which extends up to $r \approx 6.5$ nm. After this region, the density profile decays. This behavior corresponds to a layer with only a partial and fluctuating presence of fragments of BSA proteins, which extends up to long distances, of about $r \approx 10$ nm. Therefore, the thickness of the compact layer of adsorbed BSA can be estimated to be about 3 nm (from r = 3–3.5 to r = 6.5 nm), in agreement with the experimental estimate shown in Table 1.

These experimental and theoretical results strongly support the formation of a BSA monolayer of about ten molecules. BSA molecules seems to adhere to the surface of C-SPIONs with a triangular base ("side on" adsorption) since adsorption on the "side up" of BSA would give us a protein thickness on the C-SPIONs of 8 nm rather than the detected value of 3 nm (Table 1).[6,33] The "side on" adsorption of BSA expose positives patches of BSA, such as lysine and arginine amino acids and it could facilitate its tight binding.[34,35] The adsorption of BSA in the "side on" fashion was previously reported for other NPs.[36]

Conformational change of BSA upon adsorption on C-SPIONs' surface

By taking advantage of the optical properties of the aromatic residues (Phe, Tyr, Trp) of the BSA we evaluated any possible structural change that BSA underwent upon interaction with SPIONs, using UV-vis, fluorescence, synchronous fluorescence, and circular dichroism spectroscopy. Those results were also complemented with MD simulations at atomistic resolution.

The UV-vis spectrum of BSA displays two characteristic adsorption peaks: at 210 nm (related to the polypeptide backbone of the BSA) and at 280 nm (due to the aromatic amino acid residues such as Trp, Tyr, and Phe). Changes in the UV-vis spectra are indicative of the interaction of BSA with the SPIONs.[37] In our case the peak at 210 nm undergoes a red shift with increasing concentration of C-SPIONs (Fig. 4a), which reflects the modification of the polypeptide framework of the protein,[38] while the peak at 280 nm blue-shifts, indicating that the aromatic residues of the protein are exposed to a more polar microenvironment.[39,40]

Trp, Tyr, and Phe are intrinsic fluorophores whose fluorescence is susceptible of quenching upon changes in the microenvironment of the residues;[41] this allows us to investigate the interaction mechanism of BSA and SPIONs.[37,42,43] Trp is the residue that contributes most to the intrinsic fluorescence of the protein since Phe has a low quantum yield and Tyr is quenched by neighboring chemical groups under an excitation wavelength of 295 nm. BSA has two Trp residues; Trp213 and Trp134, which are in the hydrophobic loop and hydrophilic region, respectively (Scheme 1). If BSA adsorption on the surface of C-SPIONs occurs in regions close to the Trp residues, perturbations in the fluorescence spectra intensity and maximum emission wavelength (λ_{max}) appear (Fig. 4b).[42,44]

On selective excitation of the Trp residues at 295 nm, we observed a decrease of the fluorescence emission intensity at approximately 350 nm, which indicates quenching of C-SPIONs on BSA.[37,39,45] The small red shift of λ_{max} from 350.5 to 355.5 nm indicates some structural modification of BSA (Fig. 4b). C-SPIONs did not fluoresce when excited at 295 nm (Fig. S5†). By using the Stern–Volmer function (eqn (2)) we analyzed the quenching mechanism that C-SPIONs exert on the protein.

$$\frac{F_0}{F} = 1 + K_q\,\tau_0[\text{C-SPIONs}] = 1 + K_{SV}\,[\text{C-SPIONs}] \quad (2)$$

$$K_q = K_{SV}/\tau_0 \quad (3)$$

where F_0 and F are the fluorescence intensities of BSA excited at 295 nm in the absence and presence of the quenching C-SPIONs. A linear Stern–Volmer plot allows us to compute the Stern–Volmer constant K_{SV} (M^{-1}) by determining the quenching efficiency of the quencher, while K_q (eqn (3)) is the quenching constant (M^{-1} s^{-1}) and τ_0 is the mean fluorescence lifetime of the fluorophore in the absence of quencher (τ_0 for BSA = 5×10^{-9} s);[46] Fig. S6.†

Quenching mechanisms are classified in two types: static and dynamic, depending on the K_q value. The static mechanism ($K_q > 2 \times 10^{10}$ M^{-1} s^{-1}) indicates the formation of a protein–quencher complex due to the strong interaction of proteins with the quencher, whereas dynamic quenching ($K_q < 2 \times 10^{10}$ M^{-1} s^{-1}) implies a weak interaction between proteins and the quencher without stable complex formation.[47] In our case, the value of $K_q = 7 \times 10^{12}$ M^{-1} s^{-1} indicates a static quenching mechanism, which confirms the formation of BSA-SPION complexes and a strong interaction between BSA and C-SPIONs. Additionally, the binding constant K_a and the number of binding sites n of the BSA-SPIONs complex can be determined by using eqn (4).[48]

$$\log\frac{F_0 - F}{F} = \log K_a + n\,\log[\text{C-SPIONs}] \quad (4)$$

Table 1 Comparison of the thickness of the saturated BSA monolayer and the saturated number of BSA molecules per SPION, as determined by different analytical methods

Method	$r_{SPIONs+BSA}$ (nm)	r_{SPIONs} (nm)	Thickness of the BSA monolayer (nm)	N (saturation number of BSA molecule per SPION)
TEM[a]	6	3	3 ± 1[b]	10 ± 2[c]
UV-vis				10
MD simulation	≈6.5	3	*ca.* 3–3.5	10

[a] BSA-SPIONs were negatively stained by using uranyl acetate before TEM measurement, for a better visual image of the BSA shell. [b] Thickness determined in a dry state. [c] Number determined according to the model described.

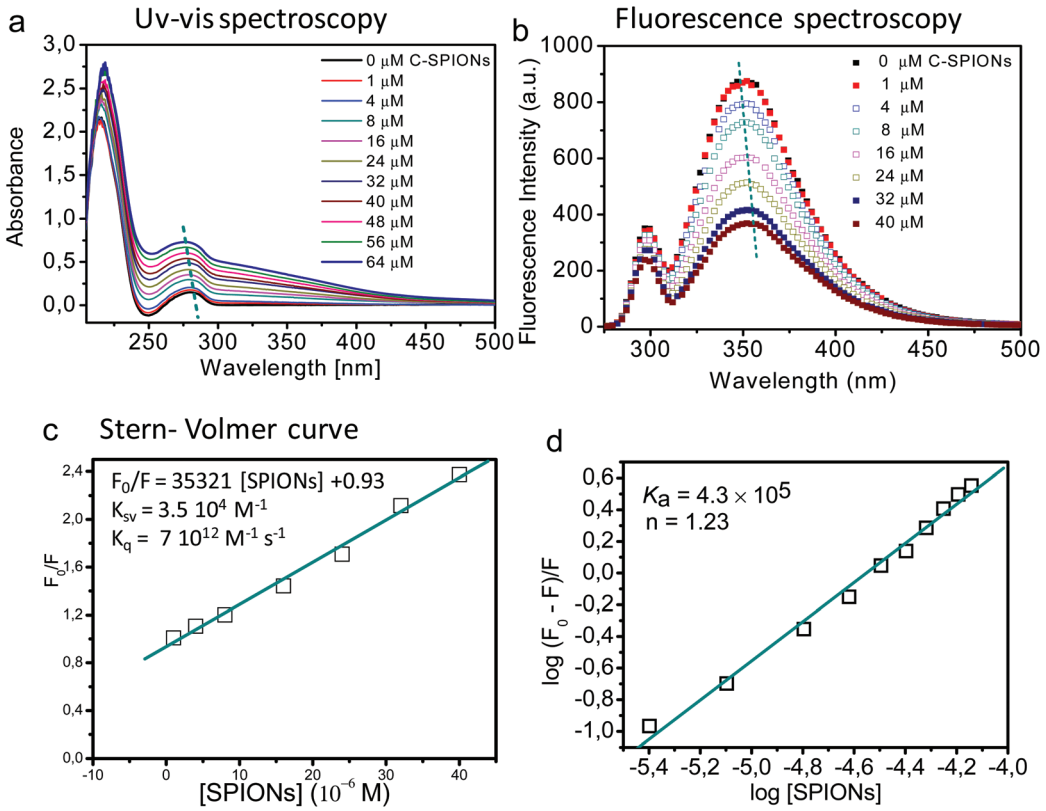

Fig. 4 (a) UV-vis spectra of 4×10^{-6} M BSA with increasing concentration of C-SPIONs at pH 7.4. C-SPIONs concentration ranges from 0–64 μM. (b) Fluorescence spectra of 4×10^{-6} M BSA with increasing concentration of C-SPIONs at pH 7.4, upon excitation at 295 nm. (c) Linear Stern–Volmer plot. (d) Determination of the binding constant, K_a, from the fluorescence measurements.

where F_0, F, and [C-SPIONs] are the same as described as in eqn (2). Here, we computed $K_a = 4.3 \times 10^5$ M^{-1}, which confirms the strong interaction between C-SPIONs and BSA.[49] The number of binding sites (n) obtained is 1.23, which indicates that there is only one type of binding site for BSA adsorption on the C-SPIONs, as mentioned above.

Synchronous fluorescence spectroscopy allows simultaneous scanning of the excitation and emission spectra of the BSA, while keeping a constant interval ($\Delta\lambda$) between them. This method provides detailed information on the microenvironment of specific aromatic amino acid residues such as Trp or Tyr. Those residues can be used to analyze the structure of the BSA due to its high content in the protein.[50] When $\Delta\lambda$ is set at 15 and 60 nm, the synchronous fluorescence spectra obtained trace characteristic information of Tyr and Trp residues, respectively.[39] Fig. 5 shows the exponential decrease in the synchronous fluorescence spectra of Tyr (287–290 nm) and Trp (279–282 nm) residues of BSA with increasing concentration of C-SPIONs. Synchronous fluorescence intensity of Trp is weaker than Tyr at $\Delta\lambda$ = 60 nm, probably due to the lower content of Trp residues than Tyr within BSA (20 Tyr residues:2 Trp residues per BSA molecule).[50] Red shifts in maximum emission wavelength (λ_{max}) are related to the protein's conformational change[51] and indicate that the residues' microenvironment becomes less hydrophobic and residues are exposed to the polar solvent; it seems conformation's BSA changes expanding and decreasing its packed structure.

Finally, the secondary structure of the supported BSA was evaluated by using circular dichroism spectroscopy (CD) and indicated the presence of two main peaks at 208 and 222 nm that are characteristic of its α-helical content. There are no changes in the α-helical content of BSA and only a slight decrease in the β-strand is detected, Fig. 5d and Table S2.† This result indicates that BSA adheres to the SPIONs surface and modifies its hydrophobic/hydrophilic regions without significantly affecting the main secondary structure native features of BSA.

We studied the possible conformational changes during BSA adsorption in our MD simulations. The most significant changes occur during the adsorption of a BSA protein onto an initially empty NP. This process can be seen in movie S1.† Three snapshots of the process are also shown in Fig. 6. These snapshots represent three different stages in the BSA adsorption process. Initially, the BSA protein moves from bulk solution to touch the NP surface (Fig. 6a). Then, the protein spreads out over the NP, increasing the contact region between the protein and the NP (Fig. 6b). Finally, the protein relaxes its conformation into a more compact configuration (Fig. 6c). These changes were characterized by computing the solvent accessible surface area (SASA), the root-mean-square deviation

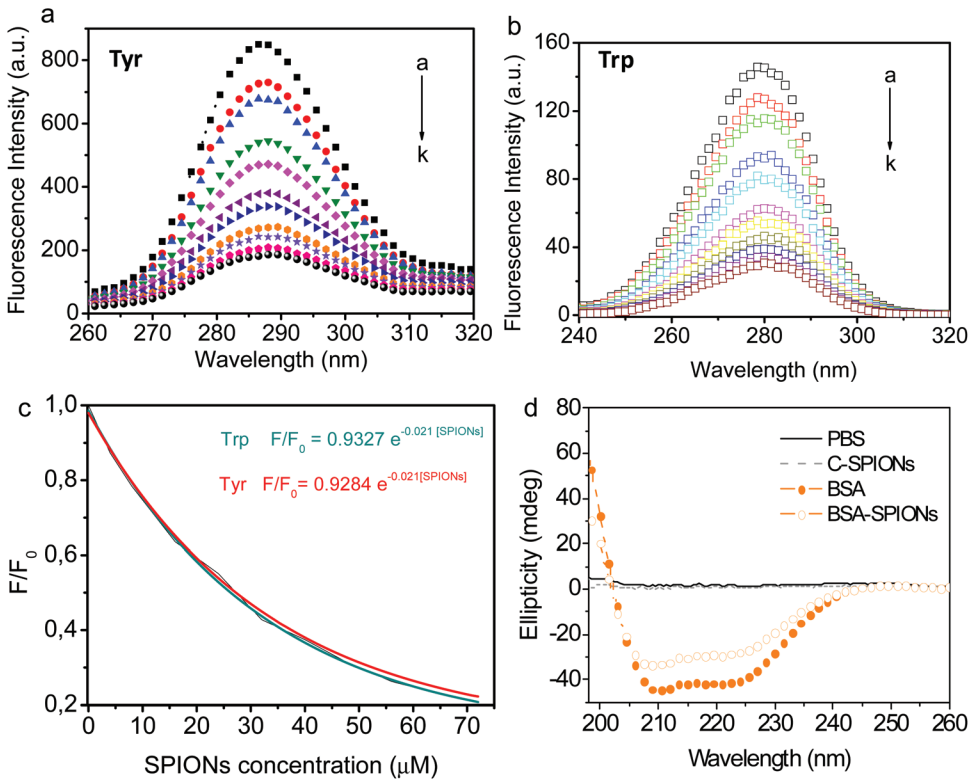

Fig. 5 Synchronous fluorescence spectra of 4×10^{-6} M BSA for (a) $\Delta\lambda$ = 15 nm (Tyr), (b) $\Delta\lambda$ = 60 nm (Trp) upon increasing concentration of C-SPIONs. C-SPION concentration is from 0–72 μM (curves a–k). (c) Ratio of synchronous fluorescent intensity (F/F_0) of 4×10^{-6} M BSA in the presence of increasing SPION concentrations for $\Delta\lambda$ = 15 nm. (d) CD spectra of PBS, C-SPIONs, BSA, and BSA-SPIONs with a BSA concentration of 4×10^{-6} M.

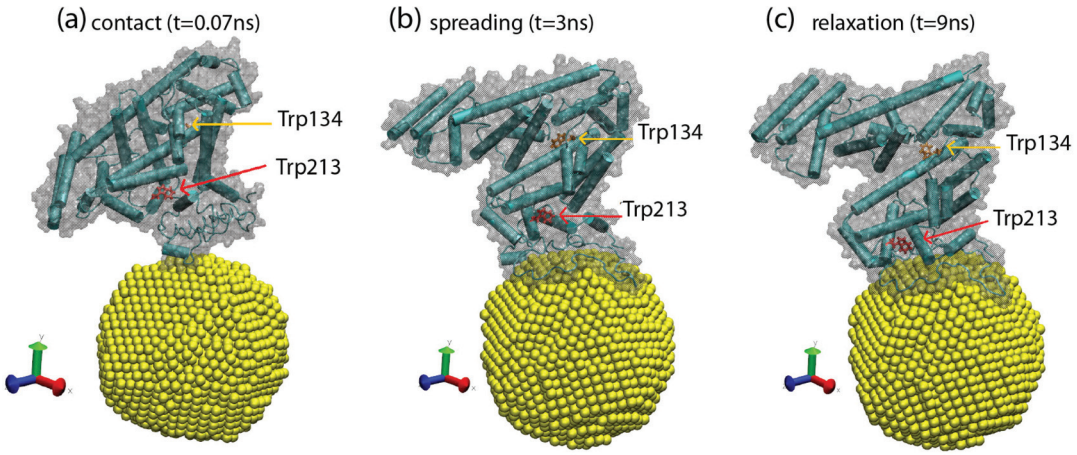

Fig. 6 Snapshots from MD simulations obtained by using VMD software,[26] corresponding to three different stages of protein adsorption. (a) Contact between BSA and the NP (t = 0.07 ns), (b) spreading of the BSA over the NP (t = 3 ns), and (c) relaxation of the adsorbed BSA protein (t = 9 ns). The NP is shown in yellow and the BSA is shown in cartoon representation, emphasizing the secondary structure. The surface of the protein is also shown as a shadow. The Trp134 and Trp213 residues are shown in bond representations in red and orange, respectively.

of atomic positions (RMSD), and the α-helix content from the simulation trajectory, by using the VMD software.[26] As the protein contacts the NP, the SASA increases from 325.1 nm^2 in solution to 345 nm^2 at the NP surface. After adsorption, the BSA relaxes to a more compact configuration with a SASA of 334.5 nm^2 (a plot of SASA as a function of time is given in Fig. S7†). The RMSD between BSA adsorbed at the NP and BSA in solution is 5.8 $Å^2$, so globally we obtained a relatively small change in atomic coordinates of the BSA. Conformational changes of BSA tend to be rather small for adsorption onto

small NPs, such as in our case, Fig 5d and Table S2,† and substantial for particles with radii larger than around 100 nm.[3]

We also monitored the residues Trp213 and Trp134, which are responsible for the changes in the Fluorescence spectra monitored in Fig. 4b. In Fig. 6, we also see that these changes affect the local environment and orientation of the Trp213 and Trp134 residues, which suggests a direct relation with the results shown in Fig. 4. Simulations indicate a significant change in the locations of the Trp213 and Trp134 residues. For these residues, we obtain a RMSD of 4 Å^2, which mostly originates during the structural relaxation observed from Fig. 6b to c and movie S1.† This change is substantial, while the overall RMSD change in the BSA protein is 5.8 Å^2, as mentioned above.

Protein resistant activity of BSA-SPIONs

The work described so far indicates the presence of a protein monolayer coating on the C-SPIONs, which in light of XPS analysis and MD simulations is quite compact. To further confirm these findings we computed the binding affinity of BSA to C-SPIONs by isothermal titration calorimetry (ITC), measuring the enthalpy, entropy, and Gibbs free energy of the adsorption process which is exothermic, therefore enthalpically favored (Fig. 7a). To quantify the thermodynamic parameters of the BSA–SPIONs interaction, the titration curve of BSA with C-SPIONs at room temperature was fitted using a single-binding model. The enthalpy (ΔH), binding stoichiometry (N) and constant (K_a), Gibbs energy changes (ΔG) and entropy (ΔS) are summarized in Table 2.

The values of $\Delta H < 0$ and $\Delta S > 0$ indicate that electrostatic interaction is the dominant force for the formation of the BSA-SPIONs complex.[52] Although BSA and C-SPIONs are both negatively charged under the same conditions, BSA could bind by electrostatic attraction through its positive patches,[34,35] which gives $K_a = 3.22 \times 10^5$ M^{-1} in the corresponding titration. This value of K_a is remarkably similar to that measured from the fluorescence spectra, which supports the concept of a strong electrostatic interaction between BSA and the C-SPIONs.

ITC values indicate a strong interaction of BSA with the C-SPIONs, therefore we compared this interaction with that between fetal bovine serum (FBS) and C-SPIONs, which could mimic what our C-SPIONs would encounter in cell culture conditions or in intravenous injection if they are not protected with the BSA coating. We exposed C-SPIONs to FBS, and by using ITC (Fig. 7b and Table 2), we obtained the thermodynamic parameters $\Delta G < 0$, $\Delta H < 0$ and $\Delta S < 0$, $K_a = 0.36 \times 10^5$ M^{-1} and $n = 0.48 \pm 1.46$. These results indicate that the interaction of C-SPIONs and FBS is mainly due to van der

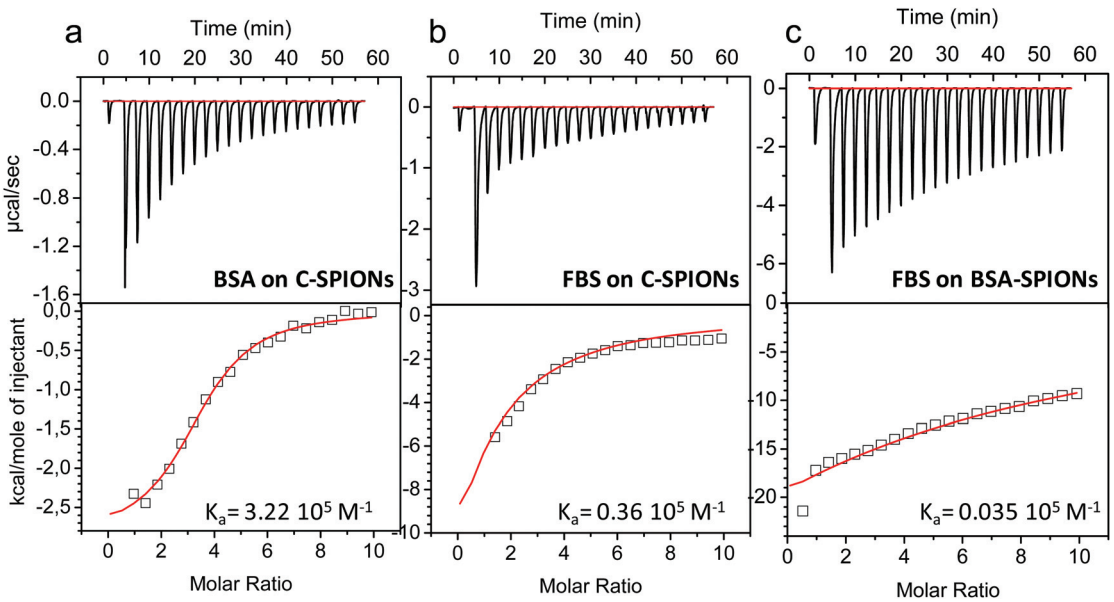

Fig. 7 ITC data for the adsorption of BSA, (a) and FBS, (b) on C-SPIONs, and (c) adsorption of FBS on BSA-SPIONs. Upper graphs present the raw data obtained from the titrations and lower graphs the integrated heats of each peak with a corresponding fitting curve.

Table 2 Thermodynamic values of BSA-SPIONs interaction derived from ITC measurements

Sample	Protein	K_a (10^5 M^{-1})	ΔG (Kcal mol^{-1})	ΔH (Kcal mol^{-1})	ΔS (cal mol^{-1} K^{-1})	N
C-SPIONs	BSA	3.22	−3.27	−2.88	15.5	3.44 ± 0.08
C-SPIONs	FBS	0.36	−66.3	−71.8	−220	0.48 ± 1.46
BSA-SPIONs	FBS	0.035	−1327.7	−1445.4	−4710	0.48 ± 3.66

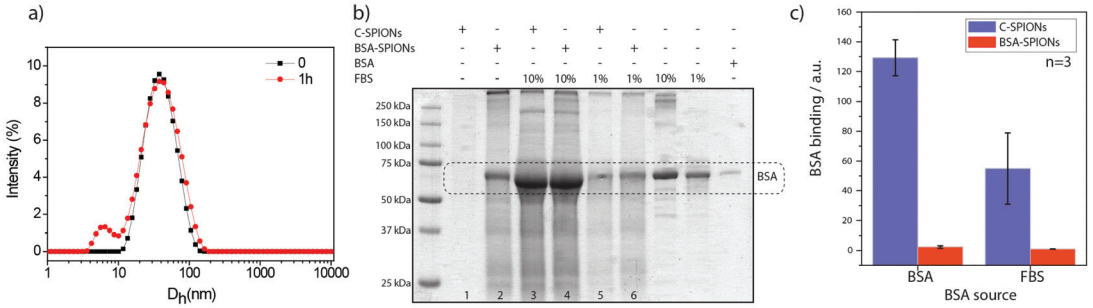

Fig. 8 (a) DLS of BSA-SPIONs at time 0 (black line) and after 1 h (red line) exposure to FBS. (b) Representative SDS-PAGE gel of C-SPIONs and BSA-SPIONs isolated from PBS containing 10% FBS, after 1 h incubation. (c) BSA binding capacity of C-SPIONs and BSA-SPIONs mixed with pure BSA or FBS determined in three SDS-PAGE gels with three independent preparations, by the ratio of the area under the curve BSA band (*ca.* 67 kDa in (b)) for lanes 3 : 1 and 5 : 1 for C-SPIONs, and 4 : 2 and 6 : 2 for BSA-SPIONs, with BSA and FBS respectively.

Waals' or hydrogen bonding,[53] with a K_a value ten times smaller than that of the K_a for BSA-SPIONs and $\Delta S > 0$.

From these results, we wondered if BSA acts as a protein-resistant coating. Therefore, we exposed BSA-SPIONs to FBS. The hydrodynamic diameter measured by DLS after 1 h exposure of BSA-SPIONs to FBS did not change, which indicates non-specific adsorption (Fig. 8a). We titrated BSA-SPIONs with FBS and we obtained $\Delta G < 0$, $\Delta H < 0$ and $\Delta S < 0$ and $K_a = 0.035 \times 10^5\ M^{-1}$, 100 times smaller than K_a for BSA-SPIONs, corroborating the strong interaction of BSA with C-SPIONs and the protein-resistant activity of preformed BSA layer against FBS, Fig. 7c and Table 2.

The protein repellency was further evaluated by means of sodium dodecyl sulfate-polyacrylamide gel electrophoresis (SDS-PAGE). We incubated C-SPIONs and BSA-SPIONs with BSA and FBS (pH 7.4) for 1 h, followed by purification with gel electrophoresis. C-SPIONs and BSA-SPIONs were used as the control. In the gel (Fig. 8b), we identified and quantified the amount of additional BSA bound to the samples. The amount of BSA bound from FBS or pure BSA to the BSA-SPIONs is negligible (Fig. 8c) compared to C-SPIONs, which bind a large amount of BSA from both pure BSA or FBS sources (Fig. 8c); this indicates that BSA shows a strong affinity to C-SPIONs' surface. When the C-SPIONs' surface is precoated by a BSA monolayer, it is unlikely that other proteins will adsorb on their surface due to the weak interaction of the BSA coating with FBS proteins. Molecular dynamics previously showed that extra molecules of BSA did not attach to the preformed monolayer of BSA, which validates the protein-resistant properties determined here.

Conclusions

Adsorption of proteins on the surface of NPs is a complex process, which depends on the physicochemical properties of the NPs, their native surface coating and the characteristics of the adsorbed proteins, as well as the nature of the medium exposed. These factors affect the amount and orientation of protein bound on the NPs' surface. Our experiments indicate that the BSA electrostatically adsorbs on citrate-coated SPIONs' surface to form a monolayer of 3 nm, which suggests the adsorption of BSA with a "side on" configuration on the C-SPIONs' surface. XPS and FTIR evidenced the presence of citrate on the BSA-SPIONs complexes. By using TEM, UV-vis, and molecular dynamics we determined that the monolayer of BSA is composed of ten molecules of BSA.

By taking advantage of the intrinsic fluorescence of aromatic residues (Phe, Tyr, Trp) of the BSA we studied its conformational changes. UV-vis, fluorescence and synchronous fluorescence spectroscopies indicated that the regions close to Tyr and Trp are perturbed upon interaction with SPIONs and undergo a decrease in hydrophobicity that induces slight changes in the BSA conformation. CD also indicated a slight change in the BSA conformation which suggests that these polar changes could be localized close to the regions of Tyr and Trp and do not affect the overall secondary structure of the BSA. By using Stern–Volmer law we determined a single-binding-site binding mechanism, a static-quenching mechanism ($K_q = 7 \times 10^{12}\ M^{-1}\ s^{-1}$) and a value of $K_a = 4.3 \times 105\ M^{-1}$ that confirms the formation of a strong BSA-SPIONs complex. By using molecular dynamics we visualized how the BSA proteins approximate the surface of the NPs and accommodate ten molecules of BSA to form a robust monolayer without significant modifications of the secondary structure of BSA.

Multiple forces such as van der Waals, hydrogen bonding, electrostatic and hydrophobic interactions, the desolvation of NPs and proteins, and solvation of newly formed complexes[53] can be involved in the interaction of BSA with SPIONs. From ITC experiments, we observed that the interaction of BSA with C-SPIONs is enthalpically favored with a K_a value determined by ITC of $3.22 \times 10^5\ M^{-1}$; this is remarkably similar to the value measured from the fluorescence spectra, which supports the hypothesis of a strong electrostatic interaction between BSA and C-SPIONs.

Additionally, ITC allowed us to evaluate the competition of the BSA layer upon exposure to FBS; we observe that FBS attaches to the SPIONs surfaces through van der Waals rather than the electrostatic interactions observed for BSA, with a K_a value that is one order of magnitude smaller than for

BSA-SPIONs. SDS-PAGE results also indicate that the amount of FBS or BSA adhered on BSA-SPIONs is negligible when the SPIONs are already decorated with BSA. We conclude that the protein shell of BSA is strongly adsorbed and does not change upon exposure to FBS and therefore acts as protein-resistant layer, similar to some PEGylated surfaces.

Our findings support the potential use of the BSA-SPIONs in medical applications, for example as an efficient carrier for targeted drug delivery *in vivo*. The preformed BSA monolayer serves as a protective shell for the SPIONs' surface and the protein-resistant surface of BSA-SPIONs avoids the adsorption of additional serum proteins, hence potentially protecting and maintaining the targeting ability of the ligands adsorbed on the NP's surface.

Acknowledgements

The research leading to these results has received funding from; the People Program (Marie Curie Actions) of the EC 7th Framework Program under grant agreement no 303630 and co-funded by the European Social Fund, the Spanish Ministry of Economy MAT2015-64442-R, co-supported by FEDER funds, the Generalitat de Catalunya 2014SGR213, the COST Action MP1202, Severo Ochoa Program (SEV-2015-0496) co-funded by European Social Funds, Ramon y Cajal grant RYC-2010-06082 (AL) and the China Scholarship Council fellowship (SMY, 201206150053). CM thanks the Innovation R&D Programme of the UK National Measurement System. AP-M is a recipient of the Universitat Autònoma de Barcelona-Programa Banco de Santander Fellowship. JF acknowledges the CESGA Supercomputing Center (Finisterrae Supercomputer) for computing time and technical assistance and proyecto de excelencia CTS-6270 de la Junta de Andalucía. We acknowledge the support of the publication fee by the CSIC Open Access Publication Support Initiative through its Unit of Information Resources for Research (URICI).

References

1 R. A. Petros and J. M. DeSimone, *Nat. Rev. Drug Discovery*, 2010, **9**, 615–627.
2 M. De, P. S. Ghosh and V. M. Rotello, *Adv. Mater.*, 2008, **20**, 4225–4241.
3 P. Satzer, F. Svec, G. Sekot and A. Jungbauer, *Eng. Life Sci.*, 2016, **16**(3), 238–246.
4 T. Sen, K. K. Haldar and A. Patra, *J. Phys. Chem. C*, 2008, **112**, 17945–17951.
5 R. Venerando, G. Miotto, M. Magro, M. Dallan, D. Baratella, E. Bonaiuto, R. Zboril and F. Vianello, *J. Phys. Chem. C*, 2013, **117**, 20320–20331.
6 M. Lundqvist, J. Stigler, G. Elia, I. Lynch, T. Cedervall and K. A. Dawson, *Proc. Natl. Acad. Sci. U. S. A.*, 2008, **105**, 14265–14270.
7 M. Lundqvist, J. Stigler, T. Cedervall, T. Berggard, M. B. Flanagan, I. Lynch, G. Elia and K. Dawson, *ACS Nano*, 2011, **5**, 7503–7509.
8 M. P. Monopoli, C. Aberg, A. Salvati and K. A. Dawson, *Nat. Nanotechnol.*, 2012, **7**, 779–786.
9 D. Walczyk, F. B. Bombelli, M. P. Monopoli, I. Lynch and K. A. Dawson, *J. Am. Chem. Soc.*, 2010, **132**, 5761–5768.
10 B. Pelaz, P. del Pino, P. Maffre, R. Hartmann, M. Gallego, S. Rivera-Fernández, J. M. de la Fuente, G. U. Nienhaus and W. J. Parak, *ACS Nano*, 2015, **9**, 6996–7008.
11 Y. Zhang, N. Kohler and M. Q. Zhang, *Biomaterials*, 2002, **23**, 1553–1561.
12 J. Xie, C. Xu, N. Kohler, Y. Hou and S. Sun, *Adv. Mater.*, 2007, **19**, 3163–3166.
13 S. Hak, E. Helgesen, H. H. Hektoen, E. M. Huuse, P. A. Jarzyna, W. J. M. Mulder, O. Haraldseth and C. d. L. Davies, *Langmuir*, 2012, **6**, 5648–5658.
14 F. Kawai, T. Kimura, M. Fukaya, Y. Tani, K. Ogata, T. Ueno and H. Fukami, *Appl. Environ. Microbiol.*, 1978, **35**, 679–684.
15 R. Gref, M. Luck, P. Quellec, M. Marchand, E. Dellacherie, S. Harnisch, T. Blunk and R. H. Muller, *Colloid Surf., B*, 2000, **18**, 301–313.
16 V. Kalidasan, X. L. Liu, T. S. Herng, Y. Yang and J. Ding, *Nano-Micro Lett.*, 2016, **8**, 80–93.
17 P. Maffre, S. Brandholt, K. Nienhaus, L. Shang, W. J. Parak and G. U. Nienhaus, *Beilstein J. Nanotechnol.*, 2014, **5**, 2036–2047.
18 F. Canfarotta and S. A. Piletsky, *Adv. Healthcare Mater.*, 2014, **3**, 160–175.
19 E. Carenza, V. Barceló, A. Morancho, L. Levander, C. Boada, A. Laromaine, A. Roig, J. Montaner and A. Rosell, *Nanomedicine*, 2014, **10**, 225–234.
20 K. Hola, Z. Markova, G. Zoppellaro, J. Tucek and R. Zboril, *Biotechnol. Adv.*, 2015, **33**, 1162–1176.
21 A. Aires, S. M. Ocampo, D. Cabrera, L. de la Cueva, G. Salas, F. J. Teran and A. L. Cortajarena, *J. Mater. Chem. B*, 2015, **3**, 6239–6247.
22 S.-M. Yu, A. Laromaine and A. Roig, *J. Nanopart. Res.*, 2014, **16**, 1–15.
23 C. Louis-Jeune, M. A. Andrade-Navarro and C. Perez-Iratxeta, in *Proteins: Structure, Function, and Bioinformatics*, Wiley Subscription Services, Inc., A Wiley Company, 2012, vol. 80, ch. 374, pp. 374–381.
24 A. D. MacKerell, D. Bashford, M. Bellott, R. L. Dunbrack, J. D. Evanseck, M. J. Field, S. Fischer, J. Gao, H. Guo, S. Ha, D. Joseph-McCarthy, L. Kuchnir, K. Kuczera, F. T. K. Lau, C. Mattos, S. Michnick, T. Ngo, D. T. Nguyen, B. Prodhom, W. E. Reiher, B. Roux, M. Schlenkrich, J. C. Smith, R. Stote, J. Straub, M. Watanabe, J. Wirkiewicz-Kuczera, D. Yin and M. Karplus, *J. Phys. Chem. B*, 1998, **102**, 3586–3616.
25 A. Bujacz, K. Zielinski and B. Sekula, in *Proteins: Structure, Function, and Bioinformatics*, 2014, vol. 82, pp. 2199–2208.
26 W. Humphrey, A. Dalke and K. Schulten, *J. Mol. Graphics*, 1996, **14**, 33–38.

27 J. C. Phillips, R. Braun, W. Wang, J. Gumbart, E. Tajkhorshid, E. Villa, C. Chipot, R. D. Skeel, L. Kalé and K. Schulten, *J. Comput. Chem.*, 2005, **26**, 1781–1802.
28 D. E. Tanner, K.-Y. Chan, J. C. Phillips and K. Schulten, *J. Chem. Theory Comput.*, 2011, **7**, 3635–3642.
29 C. Calero, J. Faraudo and D. Bastos-González, *J. Am. Chem. Soc.*, 2011, **133**, 15025–15035.
30 N. A. Belsey, A. G. Shard and C. Minelli, *Biointerphases*, 2015, **10**, 019012.
31 X. M. He and D. C. Carter, *Nature*, 1992, **358**, 209–215.
32 K. M. Au and S. P. Armes, *ACS Nano*, 2012, **6**, 8261–8279.
33 T. Cedervall, I. Lynch, S. Lindman, T. Berggard, E. Thulin, H. Nilsson, K. A. Dawson and S. Linse, *Proc. Natl. Acad. Sci. U. S. A.*, 2007, **104**, 2050–2055.
34 S. H. Brewer, W. R. Glomm, M. C. Johnson, M. K. Knag and S. Franzen, *Langmuir*, 2005, **21**, 9303–9307.
35 M. L. Quillin and B. W. Matthews, *Acta Crystallogr., Sect. D: Biol. Crystallogr.*, 2000, **56**, 791–794.
36 P. Maffre, K. Nienhaus, F. Amin, W. J. Parak and G. U. Nienhaus, *Beilstein J. Nanotechnol.*, 2011, **2**, 374–383.
37 W. Hai-Dong, N. Catherine Hui, Y. Qiaoqin and B. Ildiko, *Nanotechnology*, 2011, **22**, 145703.
38 Y. Liu, F. Ji and R. Liu, *Nanotoxicology*, 2013, **7**, 97–104.
39 B. K. Paul, K. Bhattacharjee, S. Bose and N. Guchhait, *Phys. Chem. Chem. Phys.*, 2012, **14**, 15482–15493.
40 Y.-J. Hu, Y. Liu, Z.-B. Pi and S.-S. Qu, *Bioorg. Med. Chem.*, 2005, **13**, 6609–6614.
41 J. R. Albani, in *Structure and Dynamics of Macromolecules: Absorption and Fluorescence Studies*, ed. J. R. Albani, Elsevier Science, Amsterdam, 2004, pp. 141–192, DOI: 10.1016/B978-044451449-3/50004-6.
42 R. Huang, R. P. Carney, K. Ikuma, F. Stellacci and B. L. T. Lau, *ACS Nano*, 2014, **8**, 5402–5412.
43 O. K. Abou-Zied and O. I. K. Al-Shihi, *J. Am. Chem. Soc.*, 2008, **130**, 10793–10801.
44 S. Chakraborti, P. Joshi, D. Chakravarty, V. Shanker, Z. A. Ansari, S. P. Singh and P. Chakrabarti, *Langmuir*, 2012, **28**, 11142–11152.
45 Q. Yang, J. Liang and H. Han, *J. Phys. Chem. B*, 2009, **113**, 10454–10458.
46 Q. Xiao, S. Huang, Z.-D. Qi, B. Zhou, Z.-K. He and Y. Liu, *Biochim. Biophys. Acta, Proteins Proteomics*, 2008, **1784**, 1020–1027.
47 B. K. Paul and N. Guchhait, *Photochem. Photobiol. Sci.*, 2011, **10**, 980–991.
48 Z. Chi, R. Liu, Y. Teng, X. Fang and C. Gao, *J. Agric. Food Chem.*, 2010, **58**, 10262–10269.
49 N. Wang, L. Ye, F. Yan and R. Xu, *Int. J. Pharm.*, 2008, **351**, 55–60.
50 N. G. Zhdanova, E. A. Shirshin, E. G. Maksimov, I. M. Panchishin, A. M. Saletsky and V. V. Fadeev, *Photochem. Photobiol. Sci.*, 2015, **14**, 897–908.
51 S. Gorinstein, I. Goshev, S. Moncheva, M. Zemser, M. Weisz, A. Caspi, I. Libman, H. Lerner, S. Trakhtenberg and O. Martín-Belloso, *J. Protein Chem.*, 2000, **19**, 637–642.
52 S. N. Khan, B. Islam, R. Yennamalli, A. Sultan, N. Subbarao and A. U. Khan, *Eur. J. Pharm. Sci.*, 2008, **35**, 371–382.
53 M. De, C.-C. You, S. Srivastava and V. M. Rotello, *J. Am. Chem. Soc.*, 2007, **129**, 10747–10753.